

Implementation of a wetting-and-drying model in simulating the Kennebec–Androscoggin plume and the circulation in Casco Bay

Huijie Xue · Yi Du

Received: 26 August 2009 / Accepted: 17 January 2010 / Published online: 9 February 2010
© Springer-Verlag 2010

Abstract A high-resolution coastal ocean model was developed to simulate the temporal/spatial variability of the Kennebec–Androscoggin (K–A) river plume and the circulation in Casco Bay. The model results agree favorably with the moored and shipboard observations of velocity, temperature, and salinity. The surface salinity gradient was used to distinguish the plume from the ambient coastal water. The calculated plume thickness suggests that the K–A plume is surface trapped. Its horizontal scales correlate well with $Q^{0.25}$, where Q is the volume discharge of the rivers. Directional spreading is affected by the wind with the upwelling favorable wind transporting the plume water offshore. Both the wind and the tide also enhance mixing in the plume. The inclusion of a wetting-and-drying (WAD) scheme appears to enhance the mixing and entrainment processes near the estuary. The plume becomes thicker near the mouth of the estuary, the outflow velocity of the plume is weaker, and the radius of the river plume shrinks. The flow field in the model run with the WAD is noisier, not only in shallow areas of Casco Bay but also in the plume and even on the shelf. We speculate that the WAD processes can affect much larger areas than the intertidal zones, especially via a river plume that feeds into a coastal current.

Keywords Circulation · Casco Bay · The Kennebec–Androscoggin rivers · Plume · Wetting and drying

Responsible Editor: Leo Oey

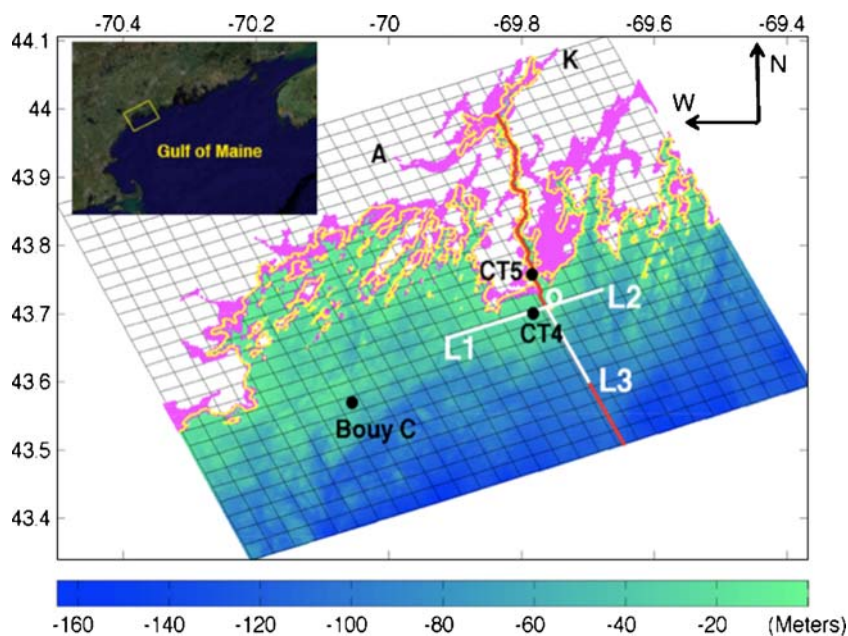
H. Xue (✉) · Y. Du
School of Marine Sciences, University of Maine,
Orono, ME 04469-5706, USA
e-mail: hxue@maine.edu

1 Introduction

Casco Bay is located in the northwestern Gulf of Maine on the western Maine coast (Fig. 1). The semidiurnal lunar tide (M_2) is the dominant tidal constituent in the bay (Parker 1982). However, the regional circulation and water properties are strongly influenced by outflows from the Kennebec and Androscoggin (K–A) rivers, the southwestward flowing Western Maine Coastal Current (WMCC) on the shelf, and the wind. For example, discharges from the K–A rivers intrude into the bay from the east, carrying excessive nutrients to the region. Observations indicate that there is a strong correlation between the salinity and the algal abundance and also suggest Casco Bay as a source region for toxic algal blooms (Keafer et al. 2005). Janzen et al. (2005) used in situ observations obtained in the spring and summer of 1998 to examine the cross-shelf flows in the eastern Casco Bay. They found that the K–A river system supplies freshwater to the eastern Casco Bay, resulting in lower salinities near the entrance. On the shelf, the along-shelf wind is important in driving the cross-shelf exchanges, whereas inside the bay, buoyancy effects and local wind are more important in forcing the currents.

This study uses a numerical model to simulate the evolution and seasonal variability of the K–A plume and how it interacts with the circulation in the Casco Bay region. There have been many studies of river plumes based on both observations and models (e.g., Chao and Boicourt 1986; Garvine 1987, 1995; O'Donnell 1990; Yankovsky and Chapman 1997; Hickey et al. 1998; Fong and Geyer 2001; Hetland 2005; Horner-Devine 2009). Following Garvine's classification (1995), the K–A plume is a large-scale plume with the Kelvin number greater than 1, for which the earth's rotational effect is important. In the absence of wind, tide, and other external forces, most of the

Fig. 1 The K–A estuary and Casco Bay (locality in the Gulf of Maine is shown as the *yellow rectangle on the insert*) model grid and topography. The model has 285×274 grid points with one in every 10 grids shown in the map. Depths below the mean sea level are shown as negative values in meters. *White lines in the map* are used to calculate the plume extensions in the alongshore direction (L1 and L2) and in the cross-shore direction (L3). The intersection (O) is where the thickness of the plume is calculated. *Black dots* indicate the locations of buoy (C) and two of the cruise stations (CT4 and CT5). The *magenta shading* represents the model calculated intertidal areas. The *yellow lines* represent the land-sea boundary in the experiment without the WAD



river water turns to the right in the northern hemisphere and develops into a plume with a water bulge near the mouth. For a plume with a large Kelvin number, downstream current is narrower and weaker than the circulation near the estuary mouth, and the bulge region of the plume is of great interest (Yankovsky and Chapman 1997).

Most river plumes, including the K–A plume, are surface trapped (Geyer et al. 2004). Yankovsky and Chapman (1997) developed a simple theory to predict the spreading and vertical structure of river plumes free of external forcing and defined the surface-advected, bottom-advected, and intermediate plume forms. Hetland (2005) used the K–A river system and the plume as an archetype to demonstrate the structures of a surface-trapped river plume. As the river water leaves the estuary, vertical mixing induced by inertial shear is strong and the plume expands while the salinity increases as a result of entrainment. The effects of wind mixing are the greatest near the plume front, where the Ekman transport in the upper layer becomes large enough to induce shear instability as described by Fong and Geyer (2001). On the other hand, the orientation and the size of plumes can be changed by the wind, tide, and ambient flow (e.g., Chant et al. 2008; Choi and Wilkins 2007; Hickey et al. 2005; Pinones et al. 2005; Fong et al. 1997). Fong et al. (1997) suggested that the alongshore wind plays an important role in controlling the cross-shore spreading of the western Gulf of Maine plume.

These studies pointed out clearly the importance of river discharges, wind, tide, and ambient flow to the plume. The US Geological Survey (USGS) streamflow record shows that discharges from the K–A rivers vary strongly from season to season. They peak in late April after spring melt, followed by a dry period in summer, then a secondary peak

in late fall. Likewise, the wind also has a strong seasonality with predominantly westerly and northwesterly winds in winter and southwesterly winds in summer. The wind is more variable in spring and the easterly wind can become dominant in May (Raineault 2006). The easterly wind is known to trigger harmful algal blooms along the Maine coast, e.g., in 2005 and 2009. The WMCC is a branch of the southwestward flowing Gulf of Maine Coastal Current (GMCC). It extends from Penobscot Bay (~100 km northeast of the study area) to Massachusetts Bay. On the average, the WMCC is stronger in spring and summer and weaker in winter, but with marked interannual variability (Pettigrew et al. 2005). In addition to the seasonal variations, both the river discharge and the wind vary with the passing weather, which drives the synoptic variability in the coastal current as well as in Casco Bay. It was found both in the observation and in the model that the WMCC strengthened in response to the northeasterly wind events in May 2005. Mixing was enhanced during these events, but the stratification was reestablished quickly after the events (Cousins et al. 2006).

The shape of the estuary can also direct the plume differently. Garvine (2001) suggested that changing the inlet channel angle or allowing very shallow depths at the coast can prevent the up-coast propagation of a plume bulge. Allowing very shallow depths in ocean models, however, requires special treatments such as the wetting-and-drying (WAD) algorithms. Driven by the tide and the wind, the movement of seawater in bays, estuaries, and inlets results in not only the up and down of the sea surface but also the back and forth of the land–water interface. The foreshore and the seabed become submerged at high water levels but are exposed at low water levels. These areas are

defined as the intertidal zone. To simulate the circulation in bodies of coastal waters that include a sizeable percentage of intertidal areas, a numerical procedure known as WAD that allows land cells to become water cells and vice versa plays an important role in modifying the circulation.

A number of approaches have been implemented in various coastal ocean and storm surge models to simulate WAD phenomena. Generally, there are two categories of methods. One is the moving boundary method, in which the coastline and the number of grid cells change with time. For example, Mendelsohn et al. (2001) used the moving boundary method to simulate the marsh inundation effects in the Cooper River Estuary. However, coastal areas with complex topography, like Casco Bay, may contain tens of segments of coastline associated with islands. It is cumbersome for the moving boundary method to trace all these land–water boundary changes. The other category is the point treatment method. The point treatment method uses a domain encompassing the largest possible wet areas and a domain wide search is performed at every time step to determine whether individual cells are wet or dry. Balzano (1998) reviewed and tested several WAD schemes in a 2D shallow water model and concluded that the exchange depth and the retention volume are two crucial variables when declaring the wet/dry status. The exchange depth determined only by water levels at cell sides often leads to nonphysical, high water levels. Including water levels at cell centers with proper weights alleviates this problem.

We use the Princeton Ocean Model (POM; Mellor 2004) for this study. The standard POM is a 3D ocean circulation model with fixed land boundaries. Different WAD schemes have been implemented in POM in recent years. Xie et al. (2004) developed a mass-conserving inundation scheme and tested it in an idealized storm surge experiment. Uchiyama (2004) simulated the tidal currents in San Francisco Bay. Oey (2005) implemented a new scheme in POM, which was used to simulate 3D processes in Cook Inlet, AK (Oey 2006; Oey et al. 2007). Among all these schemes, Oey's is the only one that deals with WAD processes in baroclinic flows and is therefore adapted for the present study. Several minor modifications have been added to make this scheme stable enough for long-term integrations.

This study is aimed at understanding the formation, evolution, and seasonal variability of the K–A plume and the circulation in the Casco Bay region. In particular, the effects of a WAD algorithm on the simulated plume and the nearby coastal circulation are examined. In Section 2, a high-resolution numerical model of the K–A estuary and Casco Bay is described. Model-data comparisons are presented in Section 3. Major discharge events and basic physical processes that control the K–A plume are discussed. In Section 4, modifications to the Oey's WAD scheme are described. Results from the WAD enabled POM

are compared with the simulation without the WAD to determine to what degree the K–A plume and the circulation in Casco Bay are affected by the inclusion of the WAD algorithm. Conclusions from this research are summarized in Section 5.

2 Model description

The POM (Mellor 2004), a 3D, fully nonlinear, free surface, finite difference ocean model with the second-order turbulence closure scheme of Mellor and Yamada (1982), was used in this study. The same base model has been adopted recently for the Gulf of Maine Ocean Observing System (GoMOOS) nowcast/forecast system (Xue et al. 2005). However, the 3–5-km resolution of the GoMOOS nowcast/forecast system is too coarse to be used to study the Casco Bay area. We therefore develop a high-resolution Casco Bay submodel nested in the GoMOOS nowcast/forecast system.

The model domain covers both the K–A estuary and Casco Bay with 285×274 curvilinear grid points in the horizontal. The resolution of ~ 300 m resolves the shoreline relatively well (Fig. 1). There are 22 vertical sigma levels with higher resolutions near the surface and the bottom. The model has three open boundaries to the east, west, and south where the momentum, temperature, and salinity are derived from the GoMOOS nowcast/forecast system. We integrated the model for the period from April 2004 to December 2005. The observed wind at GoMOOS buoy C and the National Center for Environmental Prediction North American Master Grid predicted heat fluxes are specified as the surface forcing. Daily discharges of the Kennebec and Androscoggin rivers are obtained from USGS gauge stations in North Sydney and Auburn, ME (stations 01048265 and 01059000), respectively. Both stations are about 20 km from the mouth of the rivers marked as K and A in Fig. 1. To guarantee Courant–Friedrichs–Lewy condition, the external time step is 2.5 s and the internal time step is 60 s. The model-calculated elevation, horizontal velocity, salinity, and temperature are stored every 3 h.

3 Model results

3.1 Comparison with the buoy data

GoMOOS buoy C is located near the entrance to the western Casco Bay (see Fig. 1). It is approximately 25 km southwest of the K–A estuary. Water depth at buoy C is ~ 46 m. Surface (1 m) and subsurface (20 m) salinity and temperature as well as the velocity at 2 m were recorded hourly (http://gomooos.org/data/all_measurements.html?platform=C02).

Figure 2 shows the observed and the modeled velocity at GoMOOS buoy C between April 2004 and December 2005, along with the combined discharge from the K–A rivers and the observed wind at buoy C that was used to drive the model. A 33-h, Lanczos low-pass filter was applied to remove tidal currents in the velocities. Although there were the spring and fall discharge events in 2004, the magnitude of discharge was relatively low at $\sim 1,500 \text{ m}^3 \text{ s}^{-1}$. On the contrary, 2005 was one of the wettest years in record with the spring peaks at $\sim 3,400 \text{ m}^3 \text{ s}^{-1}$ and fall peaks at $\sim 2,800 \text{ m}^3 \text{ s}^{-1}$ (Fig. 2a). The surface current responded to the discharge events most of the

time with stronger flows in the spring and fall and weaker flows in the summer. The speed at buoy C correlated relatively well with discharge events of the rivers. There were sometimes disparities between the peak discharge events and the peak speed, suggesting that some other factors also influence the coastal current. For example, the speed did not increase after the discharge events in November 2004 because the alongshore current was actually northeastward before the elevated discharge in the fall and the discharge events worked to reduce the northeastward flow. The alongshore current showed a strong tendency of

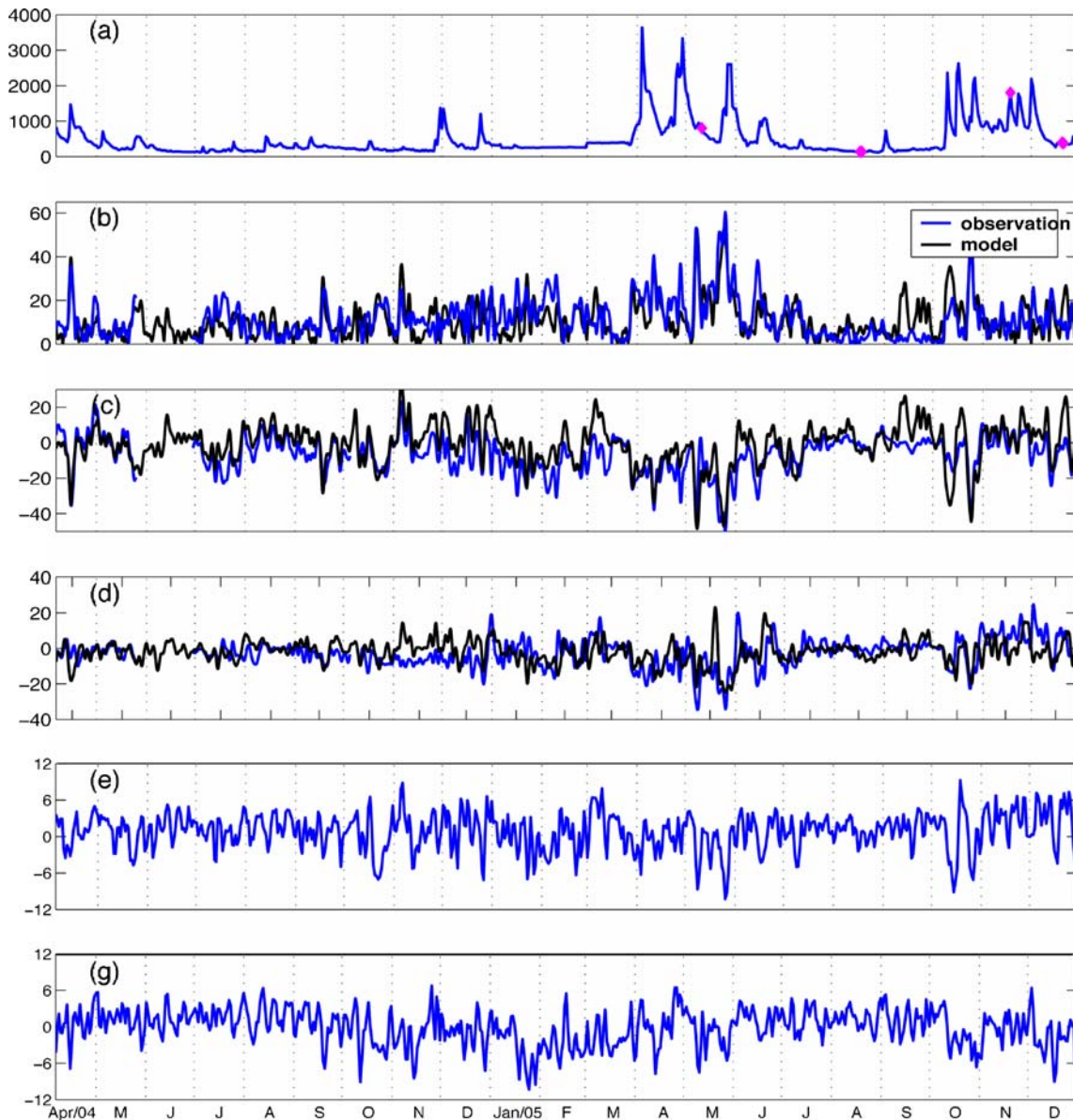


Fig. 2 Comparisons of the modeled surface current with the observations at GoMOOS buoy C. **a** The combined discharge from the K–A river system in cubic meters per second. The diamonds indicate the cruise days in Fig. 4. **b** The surface current speed in centimeters per second; **c**, **d** the alongshore and the cross-shore

velocity in centimeters per second; and **e**, **f** the alongshore and the cross-shore wind speed in meters per second, respectively. The alongshore direction defined in the model (see Fig. 1) is approximately 72° clockwise from the true north

southwestward motions induced by the plume with its strength dramatically increased after the spring freshest in both years. The cross-shore current was weaker than the alongshore current. The wind, especially the downwelling favorable wind, could intensify the surface current. For example, driven by the downwelling favorable wind on 7 and 25 May 2005, the southwestward surface current was strengthened. Overall, the modeled velocity agrees well with the observed, both in magnitude and direction.

Figure 3 shows the modeled and observed 33-h low-pass filtered time series of salinity and temperature from April 2004 to December 2005. It is obvious that the surface salinity (1 m) decreased in response to spring river discharge peaks, and the decrease lasted into the summer as freshwaters from other rivers east of the study area arrived at buoy C. Moreover, the decrease also showed large contrasts in 2004 and 2005. Freshening in 2004 occurred from April to September, and the salinity decreased by about 2. In 2005, a much wetter spring and fall (Fig. 2a) resulted in lower salinity for the year. The annual mean salinity of 2005 is lower than that of 2004 by about 1 at buoy C. The maximum decrease of salinity by about 7 was observed in April 2005 because of the stronger discharge peaks from the K–A rivers as well as lower salinities from the coastal waters upstream. The salinity variation at 20 m was much smaller compared to that at the surface but was generally lower between May and September. The plume thickness on the western Maine shelf was estimated at 10–20 m as suggested by Geyer et al. (2004), deeper in 2005 than in 2004. In addition to the seasonal freshening, the model simulated the events in both spring and fall and reproduced the 5–10-day low-salinity pulses. However, the modeled salinity was higher and the magnitudes of the low-salinity pulses were smaller than the observed ones, likely due to the higher salinity at the coastal

boundaries imported from the GoMOOS nowcast/forecast system (Xue et al. 2005).

The temperature at buoy C shows clearly the seasonal cycle. The difference between the surface and subsurface temperature reached 8°C in summer while in winter it was negligible because the vertical mixing erased the stratification. The modeled temperature compares well with the observations except from mid-January to mid-February 2005 when the water column in the model was 1~2° colder than the observations. Although the GoMOOS nowcast/forecast system assimilates the satellite derived sea surface temperature to constrain the surface heat budget, the present model relies solely on the prescribed surface and boundary fluxes and appears to overestimate the cooling in winter. Synoptic variation of temperature was particularly evident in the summer of 2005, both in the observation and in the model.

3.2 Comparison with the cruise data

Besides the buoy observations, shipboard data are also helpful in evaluating the model performance by covering large areas. A series of surveys was conducted by the Coastal Ocean Observing Center at the University of New Hampshire running between GoMOOS buoy B (43°10'50" N, 70°25' 41" W) and the K–A estuary. The part of the surveys inside of our model domain took about 4 h. Figure 4 compares the modeled salinity with the observations obtained from four cruises completed in 2005. The model simulated the salinity decrease from >30 in the coastal water to near zero in the upper estuary. Point A is defined as the plume boundary where the salinity gradient first reaches 1 km⁻¹ from west to east, which was reasonably captured in the model. Several cruises took a southeastward excursion, and the salinity always increased southeastward from the mouth towards the

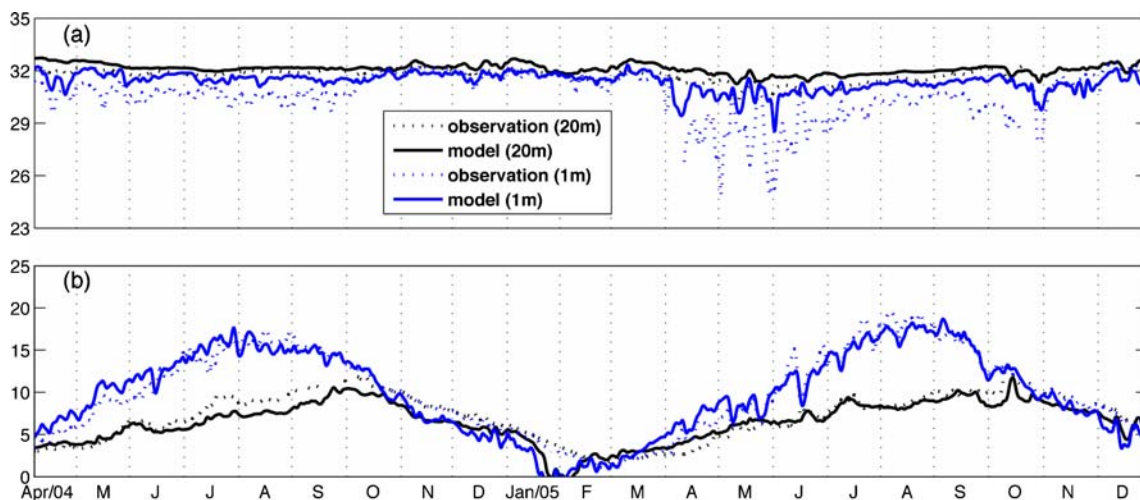


Fig. 3 Comparisons of the modeled (*solid curves*) and the observed (*dashed curves*) salinity (**a**) and temperature in degree Celsius (**b**) at GoMOOS buoy C

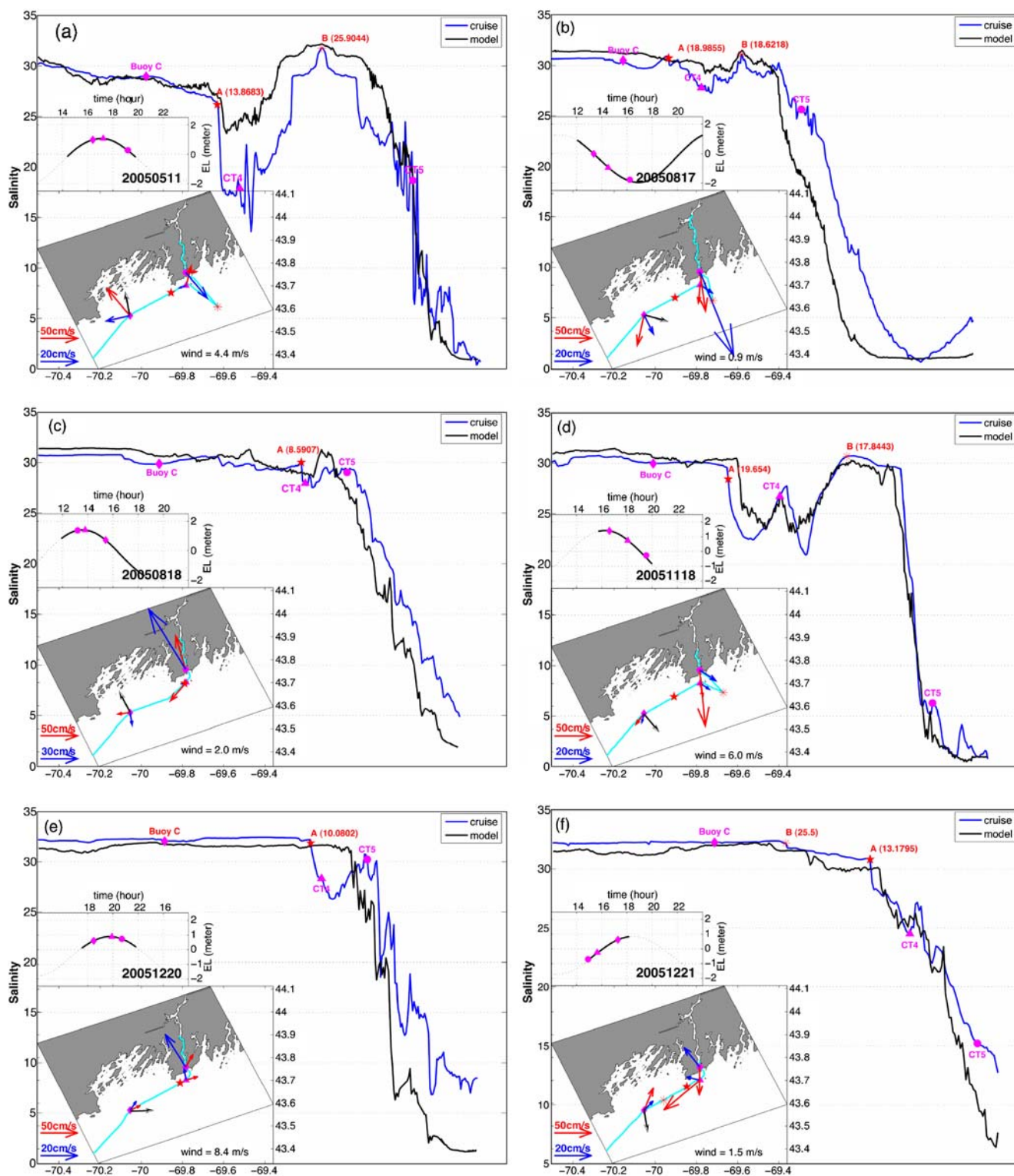


Fig. 4 Comparisons of the modeled salinity with the UNH ship survey data collected in 2005. **a, b, d, e** The eastward cruises from GoMOOS buoy B toward the K–A estuary; **c, f** the returning cruises. Magenta symbols represent the GoMOOS buoy C (diamond), coastal station CT4 (triangle), and coastal station CT5 (circular dot), respectively. *A* denotes the point where the salinity gradient (from west to east) first reaches 1 km^{-1} , and *B* denotes the maximum

southeastward excursion point during some of the cruises. The *dashed line in the upper inset* is the model elevation at buoy C and the cruise time is highlighted using the *solid line*. The cruise track is shown in the lower inset. The *black arrow on the map* indicates the observed wind direction at buoy C, while *red and blue arrows* are the modeled surface current and depth averaged current, respectively

turnaround point B. The core of the low-salinity water appeared to be sampled twice on 18 November, between A and CT4 then between CT4 and B again, both in the observation and in the model (Fig. 4d). On 20 December (Fig. 4e), a disruption in the outflow was observed so that the salinity at CT5 inside the estuary was higher than the salinity at CT4 outside the estuary. The model suggested an intrusion at CT5 at the time, but the salinity structure was not reproduced. The salinity inverse (lower at CT4 than at CT5) disappeared during the returning cruise on 21 December, for which the modeled salinity agreed well with the observed salinity.

Flows in Casco Bay and the K–A estuary are complex, and the driving forces determined by their magnitudes change over time. The effect of river discharge was overwhelming during freshets and ebbing tide as seen on 18 November (at CT4; Fig. 4d). By comparing the two back-to-back cruises in August when the river discharge was low (Fig. 4b, c), one clearly sees that the water flowed onshore/offshore during flooding/ebbing tides. Tidal currents played a significant role in determining the size of the plume. The lateral extension of the plume along the cruise tracks (measured as the distance between point A and CT4) reached 19 km at the ebbing tide (Fig. 4b) while it shrank to 8.6 km at the flooding tide (Fig. 4c).

3.3 Scales of the K–A plume

In order to characterize the K–A plume, two cross sections were taken to measure the horizontal extensions of the plume (see Fig. 1). L1 and L2 are in the alongshore direction about 2 km away from the estuarine mouth, while L3 is in the cross-shore direction. The intersection of these two cross sections is regarded as the plume center (O in Fig. 1). Although the actual center of the plume may depart from this point at any time, the displacement is usually small compared with the surface length scales of the plume.

To separate the plume water from its ambient waters, a simple method frequently used is to choose a certain isohaline (Hickey et al. 1998). Another method is to define the plume as a bulk of water mass that is more than 2 fresher than its ambient waters (Geyer et al. 2004). These definitions are based on assumptions that the plume is smaller than the area of observation/analysis and the time-independent reference salinity of the ambient waters can easily be identified. However, in this study, the K–A plume is not the only source that dilutes the coastal water. The southwestward GMCC, with its strong seasonal variability, also brings the low-salinity water from further east. It has a considerable impact on the surface salinity of the study area, from about 29 on 11 May (Fig. 4a) to 32.5 on 20 December (Fig. 4e). Regardless of the salinity of the coastal water, the salinity gradient is drastically sharper near the

plume front. This is the reason of choosing the salinity gradient threshold of 1 km^{-1} to delineate the plume water, from which the horizontal scales of the K–A plume are determined.

Time series of the alongshore and cross-shore extensions of the plume are shown in Fig. 5a, b. The rapid increases of L1, L2, and L3 appeared to follow the discharge events well, sometimes with delays. The averaged southwestward (L1), northeastward (L2), and cross-shore (L3) extensions of the K–A plume were 12, 8, and 8 km, respectively, indicating that the typical shape of the plume bulge was asymmetric in these three directions with a bias in the direction dictated by the Coriolis force. Since Casco Bay breaks the coastline, the plume often extended southwestward only for a little over 10 km before it spilled into Casco Bay. The upstream movement of the K–A plume was somewhat more prominent than expected due to the morphology of the estuary. The buoyant outflow from the estuary did not move perpendicularly to the coast. Instead, it formed an acute angle between the direction of the outflow and the upstream coastline. This outflow direction enhanced the up-coast leakage of the freshwater. Southwesterly winds, typical of the summer, also played a role in enhancing the northeastward spreading of the plume.

Within the plume water, the vertical salinity gradients are much greater than the surface horizontal gradients. As pointed out by Hickey et al. (1998), the observed maximum lateral gradient in the Columbia River plume is $\sim 1 \text{ km}^{-1}$, while the mean vertical salinity gradient within the plume is on the order of 0.25 m^{-1} . When the maximum salinity gradient was used to divide the plume from the coastal water in the vertical, the estimated plume thickness near the mouth (point O), shown as the red dotted curve in Fig. 5c, varied from about 1 m to as much as 5 m on several occasions. The thickness corresponded particularly well with L3, the cross-shore scale of the plume. Large changes in the estimated plume thickness coincided with the major discharge events. However, the physical scales of the plume (L1+L2, L3, and the thickness) during the spring freshet in the dry year of 2004 were only about 20–30% smaller than their counterparts in the wet year of 2005 although the difference in peak discharge rate between the 2 years was as large as 55%.

3.4 Factors that influence the river plume

Naturally, the amount of discharge controls the size of a plume. In addition, the wind and the tide both play important roles in affecting the state of the plume. This section focuses on the variability longer than several days using the 33-h low-passed model results, while tidal effects on the plume are examined in the next section where the experiments with and without the WAD are compared.

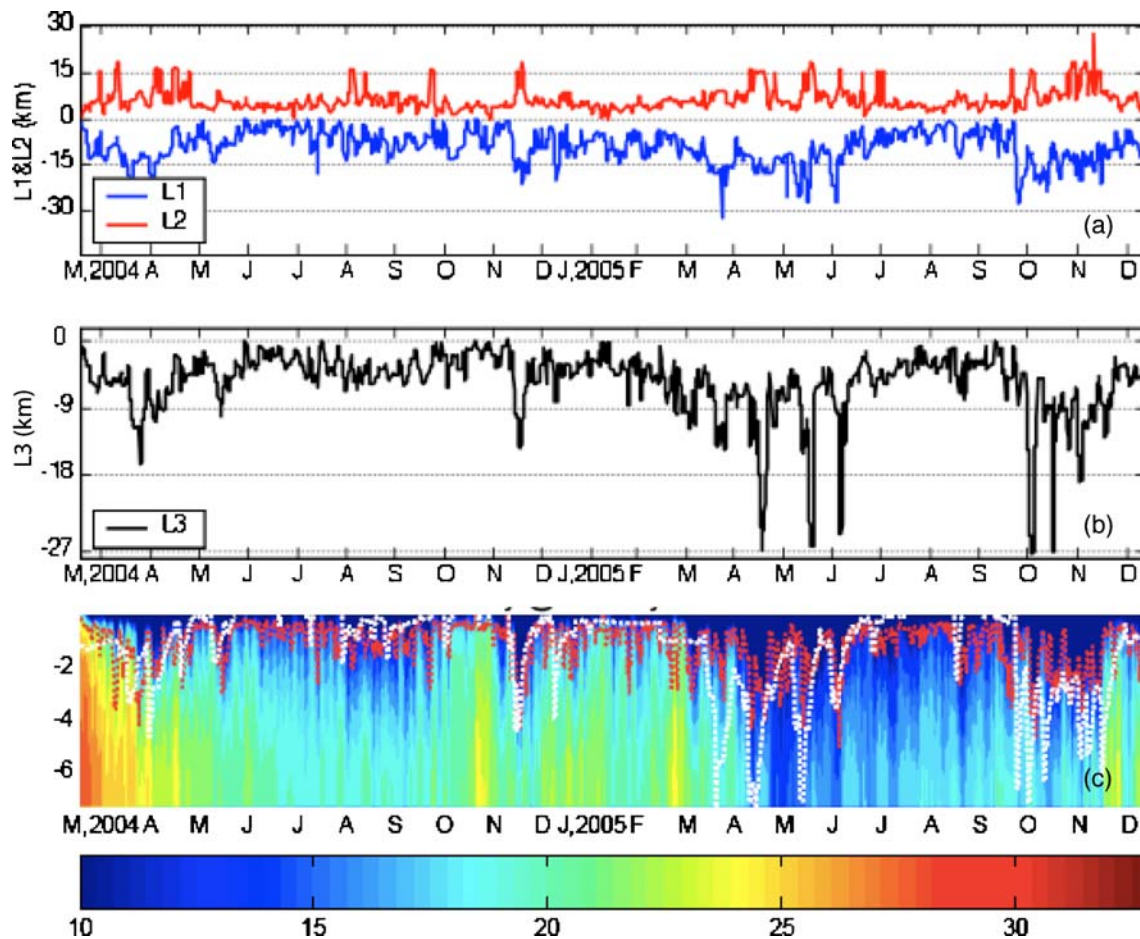


Fig. 5 The model determined plume characteristics. **a** The alongshore extensions (L1 and L2) of the surface plume in kilometers and **b** the cross-shore extension (L3) in kilometers. In **c**, the *color shading* shows the vertical distribution of salinity at point O, along with the

plume thickness as predicted by the maximum vertical salinity gradient (the *red dotted curve*). The *white dotted curve* represents the equilibrium depth defined in Section 3.4.1

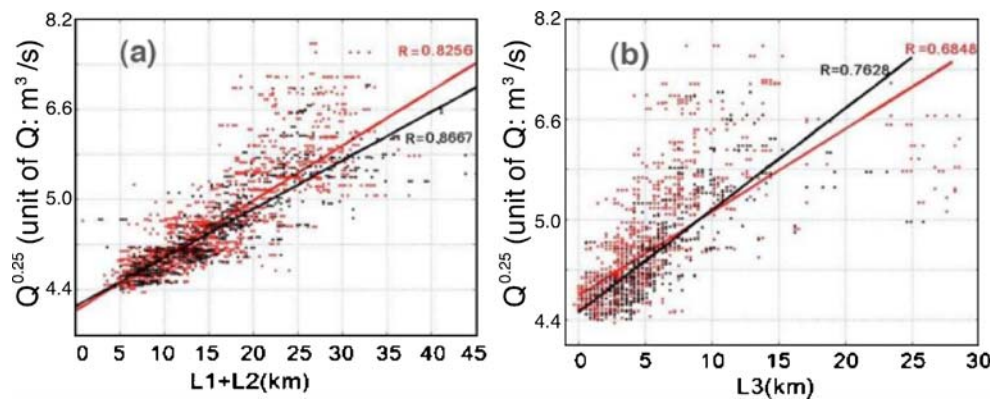
3.4.1 River discharge

In order to predict the influence of the river discharge, we first assume that the plume is driven by the river discharge and a semicircular bulge develops as suggested by Yankovsky and Chapman (1997). The entrainment occurs at the plume front, but the leakage of the plume water to the coastal water prevents the infinite growth of the plume. These two competing processes balance each other, and the volume of the plume bulge (V) is roughly proportional to the river discharge (Q). According to Yankovsky and Chapman (1997), an equilibrium depth determined by the discharge is given by $h_b = (2Q/fg')^{1/2}$. Here, Q is the volume discharge rate, f the Coriolis parameter, and g' the reduced gravity acceleration. g' can be calculated using a density difference based on the vertically averaged density in the two layers separated by the red dotted curve in Fig. 5c. The calculated equilibrium depth is shown as the white dotted curve in Fig. 5c. Because the equilibrium depth is almost

always smaller than the water depth, the K–A plume is a surface-advected plume. The volume of the semicircular bulge can then be estimated by $V = (1/3)(\pi R^2/2)h_b$, where R is the radius of the semicircular bulge at the surface. If assuming a linear relationship between V and Q , one can deduce that R is proportional to $Q^{0.25}$, similar to the conclusion of Avicola and Huq (2003) obtained from the rotating table experiments of anticyclonic plume bulges.

Using the discharge rate shown in Fig. 2a and the estimated horizontal extensions shown in Fig. 5a, b, Fig. 6 depicts the positive linear relationships between $Q^{0.25}$ and two length proxies (L1+L2 and L3), respectively. As the river discharge increases, the plume extends in all three directions. The overall correlation coefficient between the surface extensions of the plume and $Q^{0.25}$ is 0.8256 for the total alongshore extension (L1+L2) and 0.6848 for the cross-shore extension (L3), suggesting that the river discharge controls the overall evolution of the plume bulge. In particular, the plume extension in either direction alongshore

Fig. 6 Linear regression between the alongshore extension of the plume (L1+L2) and $Q^{0.25}$ (a) and between the cross-shore extension of the plume (L3) and $Q^{0.25}$ (b). Red dots represent all modeled results, while black dots show only the results when the wind speed is $<2 \text{ m s}^{-1}$



(L1 or L2), especially the upstream extension L2, is less correlated with the river discharge than the sum of L1 and L2 (Table 1). The reason is that at any given time, the plume may drift and bias toward down-coast or up-coast in response to the wind. However, the sum of the alongshore extensions, L1+L2, appears to have a tight relationship with $Q^{0.25}$. The prediction of L3 would be better if the extreme values (L3>20 km) were excluded, as deduced from Fig. 6b. This suggests that when the plume water spreads farther offshore as a result of high river discharges, impacts from the wind and the coastal current are strengthened.

There is a threshold of river discharge associated with the alongshore length of the plume. No plume is generated when the river discharge falls below the threshold since the freshwater outflow from the rivers first travels through the estuary before it enters into the sea. In our model, the discharge from the K–A river system is always greater than the threshold. This threshold is, however, invalid in the L3– $Q^{0.25}$ relationship because it is affected by the choice of the zero location (i.e., point O).

3.4.2 Winds

When the high wind (wind speed $>2 \text{ m s}^{-1}$) days are excluded from the analysis, the correlation coefficient between $Q^{0.25}$ and the two horizontal length scales, L1+L2 and L3, increases to 0.8667 and 0.7628, respectively. This illustrates the wind effects on the surface plume. The down-coast and the up-coast extension individually seem to be influenced by both the alongshore and the cross-shore wind. However, the total length (L1+L2) does not correlate with the wind (Table 1). A possible interpretation is that the wind acts to change the orientation and the center of the plume bulge while the total alongshore length of the bulge is controlled by the discharge. Table 1 also suggests that the cross-shore length of the plume is affected more by Ekman transport which is induced by the alongshore wind. Generally, northeasterly (downwelling favorable) winds limit the cross-shore extent, and conversely, southwesterly (upwelling favorable) winds push the plume farther offshore.

Note that the wind effect is determined by not only the direction but also the magnitude and the duration as described by the integral Ekman parameter $\int (\tau/\rho h f) dt$. When moderate wind changes its direction all the time as in our complex model setting, the plume may not be able to respond quickly. Moreover, the time that it takes for the river outflow from the estuary mouth to reach the front changes. Therefore, only events with more stable winds can clearly be discerned from the model result. Taking the spring freshet in 2005 for example (April to June), there were four small discharge peaks during this period. The first peak was the highest and the peaks thereafter got smaller and smaller. During the first discharge peak in early April, both the up-coast and the offshore lengths were limited, while the down-coast length reached its maximum with more than 30 km. It was the onshore wind that significantly constrained the spreading of the plume and deepened the plume. When the second discharge peak arrived in May 2005, the plume water occupied the entire water column as predicted by the equilibrium depth and the cross-shore extension was nearly doubled despite of the downwelling favorable wind.

4 Tidal effects and modifications due to the WAD

Instantaneous flow in Casco Bay is largely influenced by the semidiurnal lunar tide (Parker 1982). Tidal flats account for a sizeable percentage of the surface area at the low water. Flooding processes happening in the estuary can also

Table 1 Correlation coefficients between the horizontal extensions of the plume at the surface and the river discharge rate as well as the wind

	L1	L2	L1 + L2	L3
$Q^{1/4}$	0.7867	0.5923	0.8256	0.6848
Alongshore wind stress	0.3869	0.37	0.00907	0.221
Cross-shore wind stress	0.3235	0.3557	0.0486	0.0112

affect the formation of the river plume. As the K–A plume not only helps deliver freshwater to its nearby region but also feeds the WMCC, the influence of WAD may not be restricted to only shallow areas. The recently developed WAD algorithm by Oey (2005, 2006) is adapted for this portion of the study. The purpose is not to validate the model simulated intertidal zones, which requires a far more accurate database of shorelines. Instead, our goal is to determine the feasibility of applying the WAD for long-term simulations of the circulation in Casco Bay and the K–A estuary and to demonstrate the modifications to coastal processes when considering WAD of shallow areas.

4.1 Adaptation of the Oey’s WAD scheme

In Oey’s scheme, a minimum depth ($H_{\text{dry}}=5$ cm) was elected to determine the “dry” or “wet” state of each cell. When the total depth of a cell fell below the minimum depth, the cell was considered dry. As the POM uses C-grid, the “dry” or “wet” condition for velocity should be imposed at the cell interface. Oey (2006) proposed additional constrains to limit the anomalous flow from a dry cell to a wet cell. These treatments allow the elevation at a dry cell from the previous time step to be recalled for the next step iteration, which naturally ensures the conservation of volume. Because of the shallow depth at the wetting-and-drying interface, the velocity profile across the interface to a dry cell is assumed homogeneous to eliminate strong shears.

We have added a few minor modifications to the Oey’s WAD algorithm. In POM, the bottom drag coefficient (C_B) is given by:

$$C_B = \text{MAX} \left\{ \frac{\kappa^2}{[\ln(\{(zz(kbm1) - z(kb)) \times D\}/Z_o)]^2}, 0.0025 \right\} \quad (1)$$

where Z_o is the roughness parameter, $\kappa=0.4$ is the von Karman constant, and $(zz(kbm1)-z(kb)) \times D$ is the distance between the bottom and its nearest velocity grid point. The lower limit of 0.0025 is assigned for C_B in deep water where the bottom layer is not resolved by the model. This formula is applicable to water depths ranging from tens to thousands of meters. In waters of a few meters deep, C_B becomes very large if $[(zz(kbm1)-z(kb)) \times D]/Z_o$ approaches 1 somewhere in the domain. Mellor (2002) suggested changing the logarithmic term to $\ln\{1+[(zz(kbm1)-z(kb)) \times D]/Z_o\}$ to ensure positive values for the logarithmic term, which is adopted in the Oey’s scheme. When used in the present model configuration with 22 sigma levels, the modified formula does improve for water depths in the range of 2–4 m, but the formula still results in a bottom drag coefficient much greater than 1.0 where water depth is less than 1.5 m. We introduce a

functional form of $Z_o=0.01 \times (1-e^{-0.25D})$ in Eq. 1. The new roughness parameter represents a numerical strategy so that the C_B value is never larger than 1.0 even in extremely shallow waters while matching the original curve in deep water.

A 2D, time-dependent, masking array “WETMASK” was introduced in Oey (2005, 2006) to distinguish possible wet (WETMASK=1)/dry (WETMASK=0) cells from the absolute land areas. In Oey’s WAD scheme, the last WETMASK from the external loop was chosen as the WETMASK when calculating the internal mode. This may not be the best approximation since a cell can switch between wet and dry during the course of an internal loop. We introduce three new time-dependent masks for the internal mode (WETMASKT, DUMT, DVMT) and use the averaged quantities (ET, UTF, VTF) to recheck WAD status for the internal mode. DUMT and DVMT are masking arrays for the horizontal velocities in the C-grid, while ET, UTF, and VTF are averaged elevation and velocities over an internal time step. Finally, at dry cells, we use the vertically averaged temperature and salinity at each cell to make this thin water column have homogenous profiles. Oey (2006) suggested using the climatological salinity and temperature or air temperature at dry cells. Du (2008) found that recalling the temperature and salinity of the last wet state conserves the heat and salt in an idealized tidal mixing experiment. Moreover, the homogeneous temperature and salinity profiles in the thin layer appear to reduce numerical oscillations at the land–sea boundary.

4.2 Tidal intrusion into the estuary

To show tidal effects on the plume, the half-hourly model output of March and April 2005 is used to illustrate the back and forth movement of the plume water in the cross-shore direction (Fig. 7a, b). This period is chosen because the river discharge in March 2005 was relatively low, followed by a strong freshet in early April and another one in the end of April (Fig. 7d). The transect (the red line in Fig. 1) follows the main channel of the estuary for 45 km, and it extends offshore for 30 km to help fully trace the movement of the plume front.

A clearly semidiurnal tidal signal was obvious in both model runs, with and without the WAD. Events like strong river discharge and/or wind could modify this basic pattern, but two models responded differently to these events. In the model without the WAD, the two peak discharge events (4–7 and 24–30 April) almost destroyed the tidal pattern. A consistently seaward plume formed during the high discharge events and the coastal water did not flow into the estuary, even during the flood tide. Other events that weaken the tidal pattern were the persistent upwelling/downwelling favorable winds. The upwelling favorable

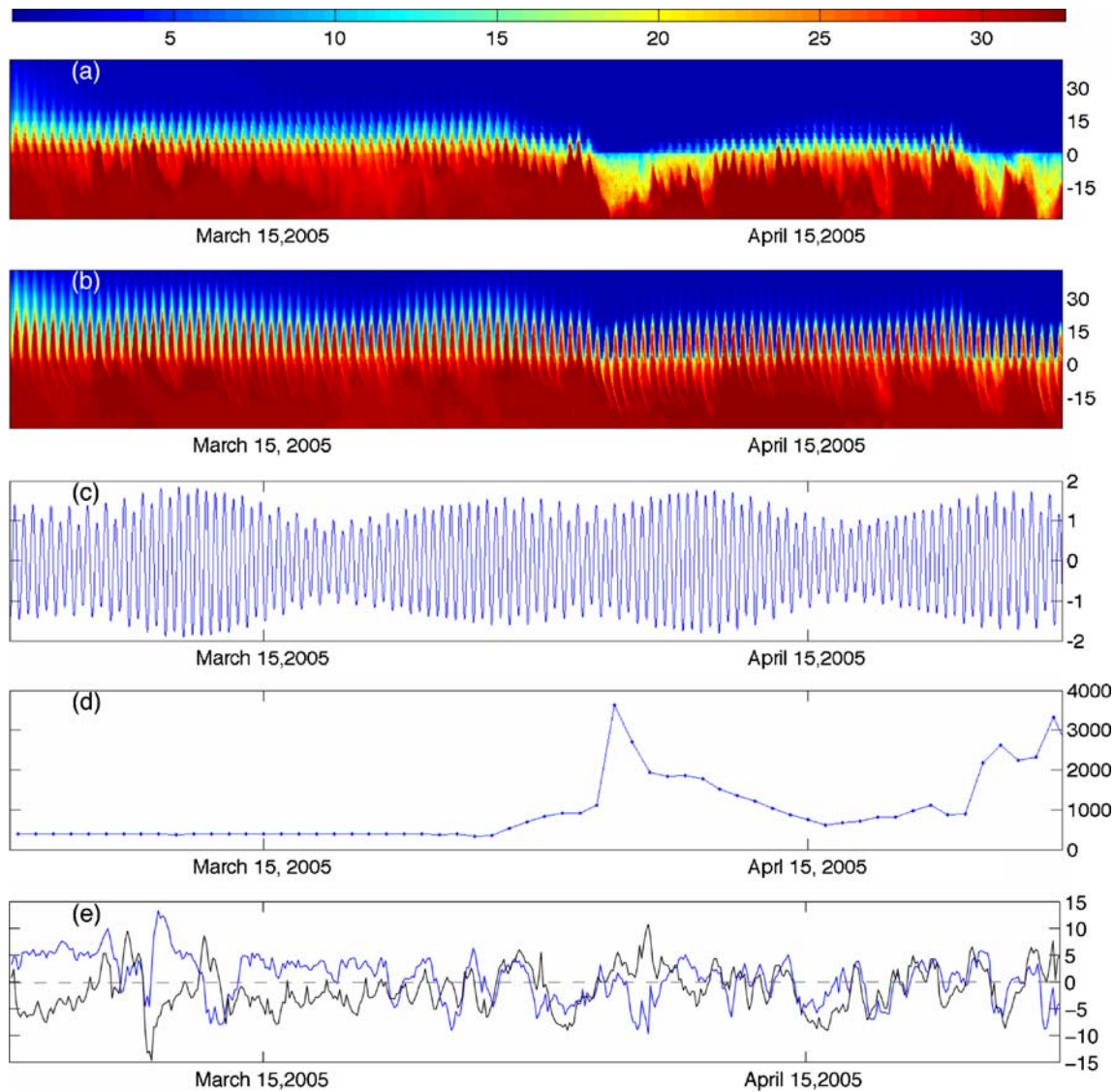


Fig. 7 The *color field* in **a** and **b** shows the surface salinity along the cross-shore transect marked as the red line in Fig. 1 in the experiment without the WAD (**a**) and in the experiment with the WAD (**b**). The reference point O (see Fig. 1) is chosen as the origin

with negative distances pointing seaward. **(c)** Shows the modeled elevation (meters) at point O, **(d)** the combined discharge from the K–A rivers in cubic meters per second, and **(e)** the alongshore (*blue line*) and cross-shore wind (*black line*) in meters per second

wind on 9 to 10 March helped in transporting the freshwater offshore. Although it was much weaker, the upwelling favorable wind persisted from 13 to 24 March except for a brief interruption on 21 March. The surface salinity offshore dropped by about 5 and the plume water almost occupied the entire transect. On the other hand, the downwelling favorable wind events in the end of March and beginning of April pushed the coastal water closer to the mouth of the estuary, even into the estuary on 2 to 3 April. Similar responses were seen in late April, driven by the consecutive downwelling favorable wind events.

The model with the WAD allows stronger tidal intrusion. The coastal water intruded more than 15 km upstream into the estuary especially in March before the arrival of spring

discharge peaks (Fig. 7b). The tidal excursion in this run matched well with the spring-neap tidal cycles seen in Fig. 7c with stronger intrusions during spring tide. This tidal rhythm was much more pronounced compared with the result from the model without the WAD. Intensified seaward extensions were also observed in the model with the WAD during the freshet events, and the salty water intrusion seemed to be impeded by the out rushing river water. However, the movement of seawater was still back and forth in the estuary, and the coastal water intrusion was clearly visible even during the peak discharge events. Modulations due to the wind events were consistent between the two experiments.

Figure 8 shows the outflow velocity and salinity at the mouth of the estuary during the peak discharge on 4 April.

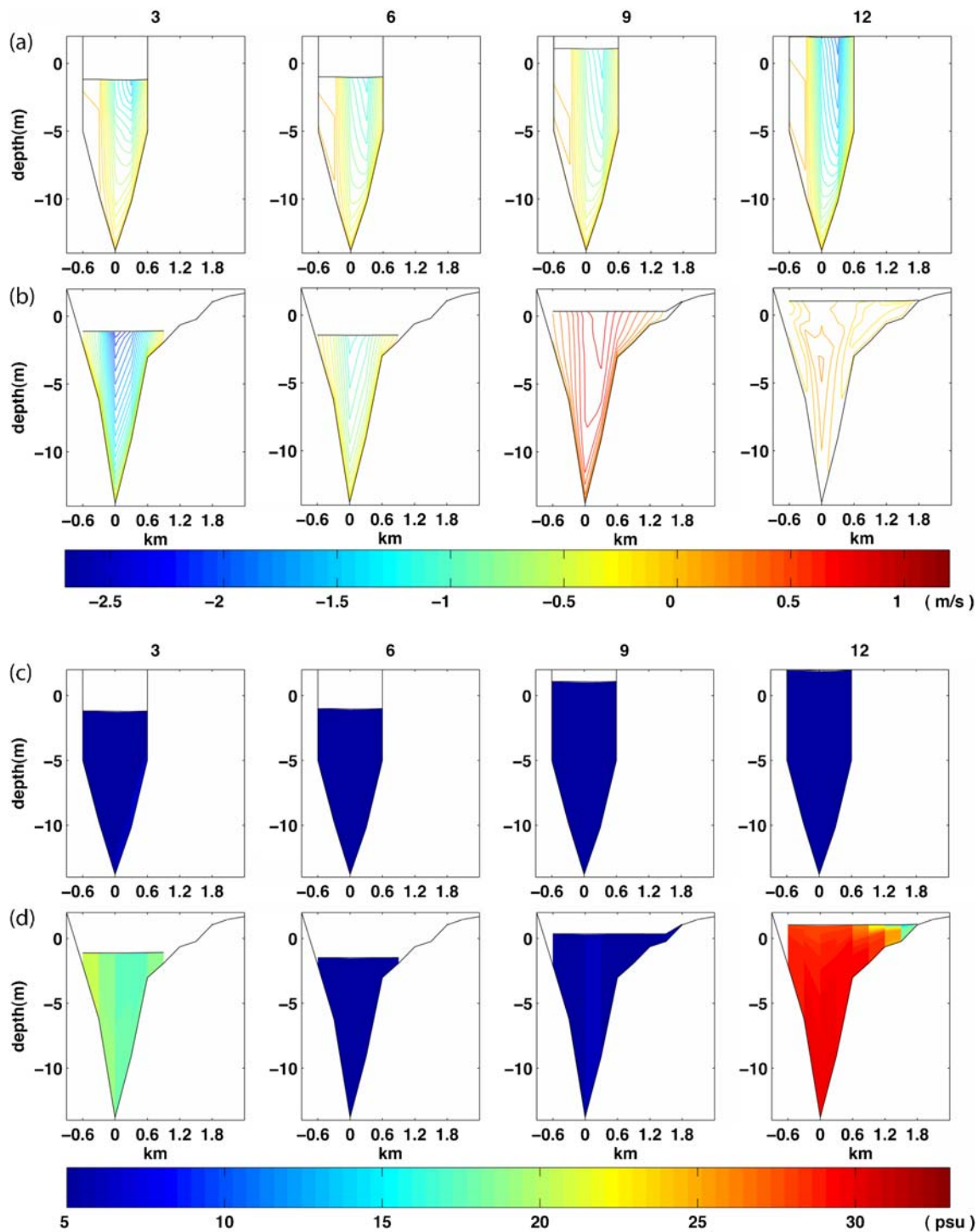


Fig. 8 Along channel velocity (**a**, **b** positives represent flows into the estuary) and salinity (**c**, **d**) near the mouth of the estuary on 4 April 2005 at 3, 6, 9, and 12 UTC for the run without the WAD (**a**, **c**) and

the run with the WAD (**b**, **d**). x -axis is the cross channel distance for a section just inside of CT5 with the origin designated as the deepest spot of the cross section

Without the WAD, the modeled outflow velocity was negative all the time, which means that the river outflow overwhelmed the flooding tidal current. Stronger flows hugged the eastern bank of the estuarine channel. The simulated salinity was less than 5 at the cross section for all

tidal phases indicating no salty water intrusion even during the flood tide. With the WAD, the velocity profile changed from negative during the ebb tide to positive during the flood tide. The outflow velocity was stronger than the inflow, as in a typical estuary. The maximum velocity was

in the center of the channel. The salinity distribution also varied dramatically during different tidal phases. The coastal water dominated whereas during the flood, during the ebb the estuary was filled with the plume water. Another significant difference was the width of the estuary. As the water flooded the shallow areas in the experiment with the WAD, the width became considerably wider at the high tide, which allowed more coastal water to enter the estuary.

4.3 The K–A plume

Figure 9 shows the K–A plume at the surface after the peak discharge on 4 April 2005. The surface area of the plume simulated without the WAD was more than twice the one simulated with the WAD. Without the WAD, the river water flowed out of the estuary and formed a large plume. The plume water extended almost equally in all directions and formed an almost semicircular bulge with a radius of

25 km. No coastal water was entrained into the plume at the surface. The low-salinity water from the previous ebb spread into Casco Bay, which lowered the salinity to less than 31 even in the western Casco Bay. With the WAD, the K–A plume was confined in a 12-km radius. The up-coast spread of the plume water was limited. This might be related to the extremely shallow depth nearshore enabled by the WAD as suggested by Garvine (2001), but it was more likely due to the enhanced entrainment and mixing that brought in and up the coastal water to result in the strain of the plume to the southeast. The western part of the plume spread toward the southeastern corner of Casco Bay and mixed with the local water mass. The plume water extended to about midbay and reduced the salinity there to about 31.

As the same amount of freshwater discharge was specified in the two model runs and the horizontal size of the plume in the WAD simulation was much smaller, the vertical extension needs to be inspected to determine if the plume was mixed more downward in the WAD simulation. Figure 10 shows the vertical distribution of salinity along a cross-shore section (see the red line in Fig. 1) at the same time as in Fig. 9. In the simulation without the WAD, the plume water extended to the bottom at the mouth, but the

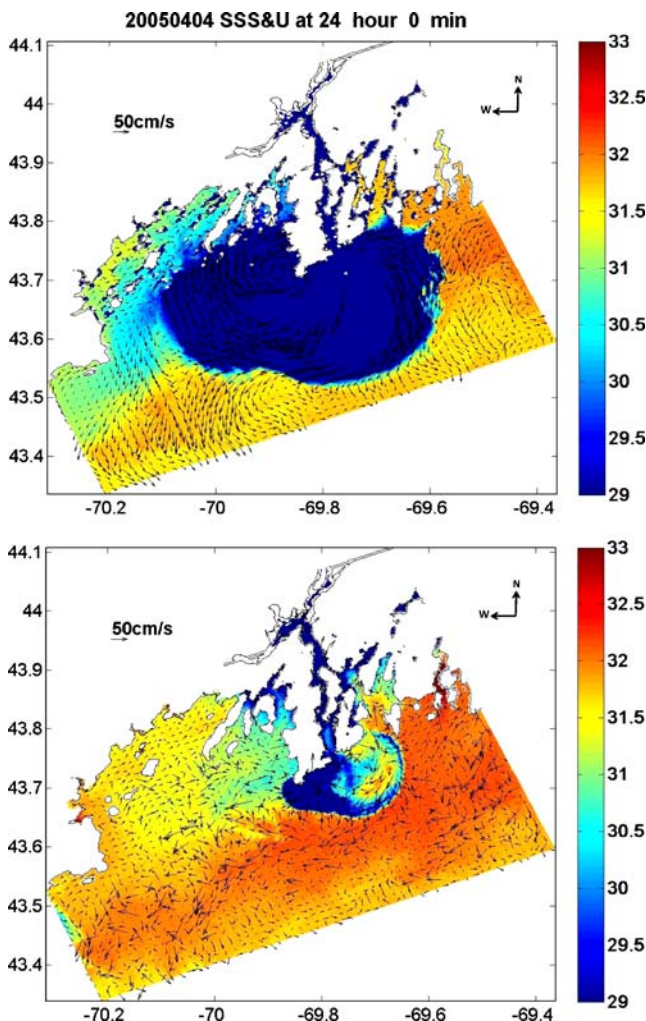


Fig. 9 The surface salinity and currents at 24:00 UTC on 4 April 2005 in the run without the WAD (*upper*) and in the run with the WAD (*lower*)

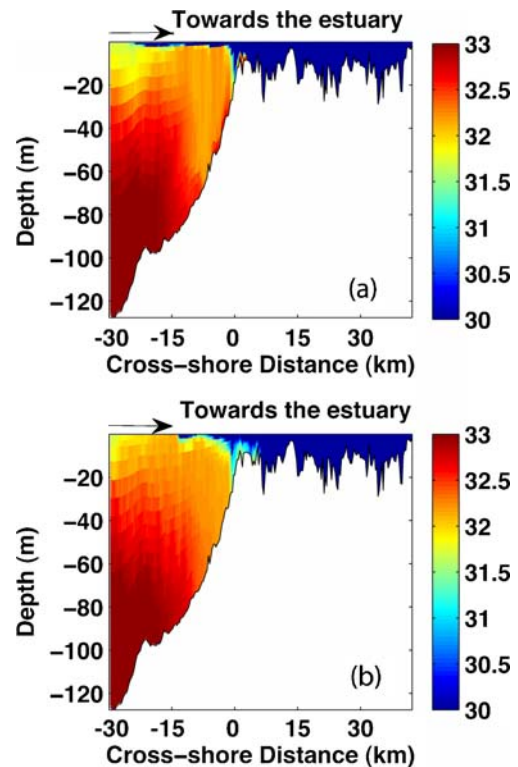


Fig. 10 Vertical distributions of salinity at 24:00 UTC on 4 April 2005 in the run without the WAD (*a*) and in the run with the WAD (*b*). The section is the same as that used in Fig. 7, i.e., the cross-shore transect marked as the red line in Fig. 1 with the origin set at point “O”

thickness reduced immediately outside so that the front was almost vertical at this location. A thin layer extended offshore to about 25 km. In the WAD run, the plume was noticeably thicker, but it was less than 15 km in the offshore direction. The front near the the mouth was slanted in the downward/up-estuary direction. Both the horizontal and vertical gradients near the front were comparatively weaker. The most likely reason is that the inclusion of WAD enhances vertical mixing near the base of the plume and the plume appears to mix downward more.

The presence of stronger mixing can also be seen in the alongshore direction of the K–A plume (Fig. 11). In the simulation without the WAD, the outflow was highly stratified near the mouth. After the plume water was transported westward for ~10 km away from the mouth, the plume began its vertical growth. Partly because the velocity was stronger on the eastern side of the estuarine channel (Fig. 8a), there was a considerable amount of eastward spreading of the plume, reaching about 15 km at the surface. In the WAD simulation, the plume was thicker near the mouth. On the western side, the plume began to grow vertically immediately after leaving the mouth, and the vertical salinity gradient was weaker, suggesting again stronger mixing in this case. The overall westward extension was ~15 km less than that in the experiment without the WAD.

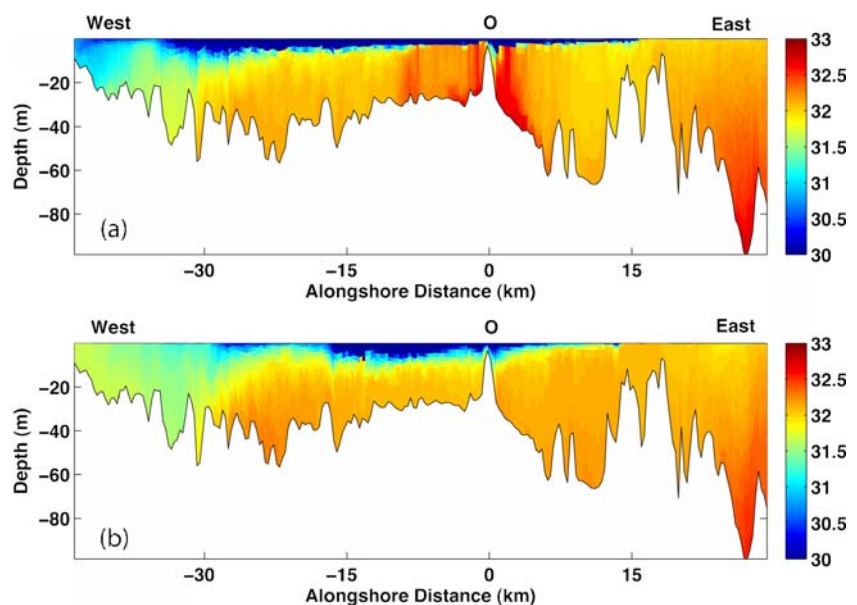
4.4 Wetting-and-drying processes

From the historical data at the water level station in Portland, ME (NOAA/NOS Station ID 8418150), the tidal range in Casco Bay is about 4 m, which generates 11,582 acres of tidal flats and 500 acres of rocky shores around Casco Bay (Casco Bay Estuary project 1995). By

implementing a WAD algorithm into our model, flooding and ebbing processes were simulated. Figure 12 compares the surface salinity and velocity between the simulations with and without the WAD during the spring tide on 9 March 2005. In order to highlight the model's ability to simulate wetting-and-drying processes, two particular times of that day are chosen: near the highest water level around 15:00 UTC and near the lowest water level around 21:30 UTC. At the highest water level, the water area was at the maximum. At the low tide, shallow areas in Casco Bay and the K–A estuary were exposed. Especially in the inner Casco Bay, intertidal zones sheltered by small islands formed tidal flats that were linked along the coastlines. Several islands, which were submerged during high tide, appeared in Casco Bay at the low tide. Also, several islands that were divided into smaller ones at the high tide connected with each other during the low tide. The model estimated total intertidal area based on the difference between the highest and the lowest water level during spring tide (see Fig. 1) was about 90 km² in Casco Bay.

The surface salinity both in the plume and in Casco Bay was fresher without implementing the WAD, consistent with the result during the high discharge period seen in Fig. 9. The plume water flowed all the way out of the estuary even during the flood tide in the simulation without the WAD. A noticeable feature in the simulation with the WAD was the saltwater intrusion into the estuary. During the flood tide, the coastal water was pumped into the estuary and formed a several kilometer long coastal water intrusion, which was perhaps why the plume on the shelf was broken to several bands. Surface currents in the shelf were mainly seaward in both model runs, driven by the strong offshore wind on 8 to 9 March followed by the

Fig. 11 Vertical distributions of salinity at 24:00 UTC on 4 April 2005 in the run without the WAD (a) and in the run with the WAD (b). The cross section is along the L1 to L2 line in Fig. 1 with the origin set at point “O”



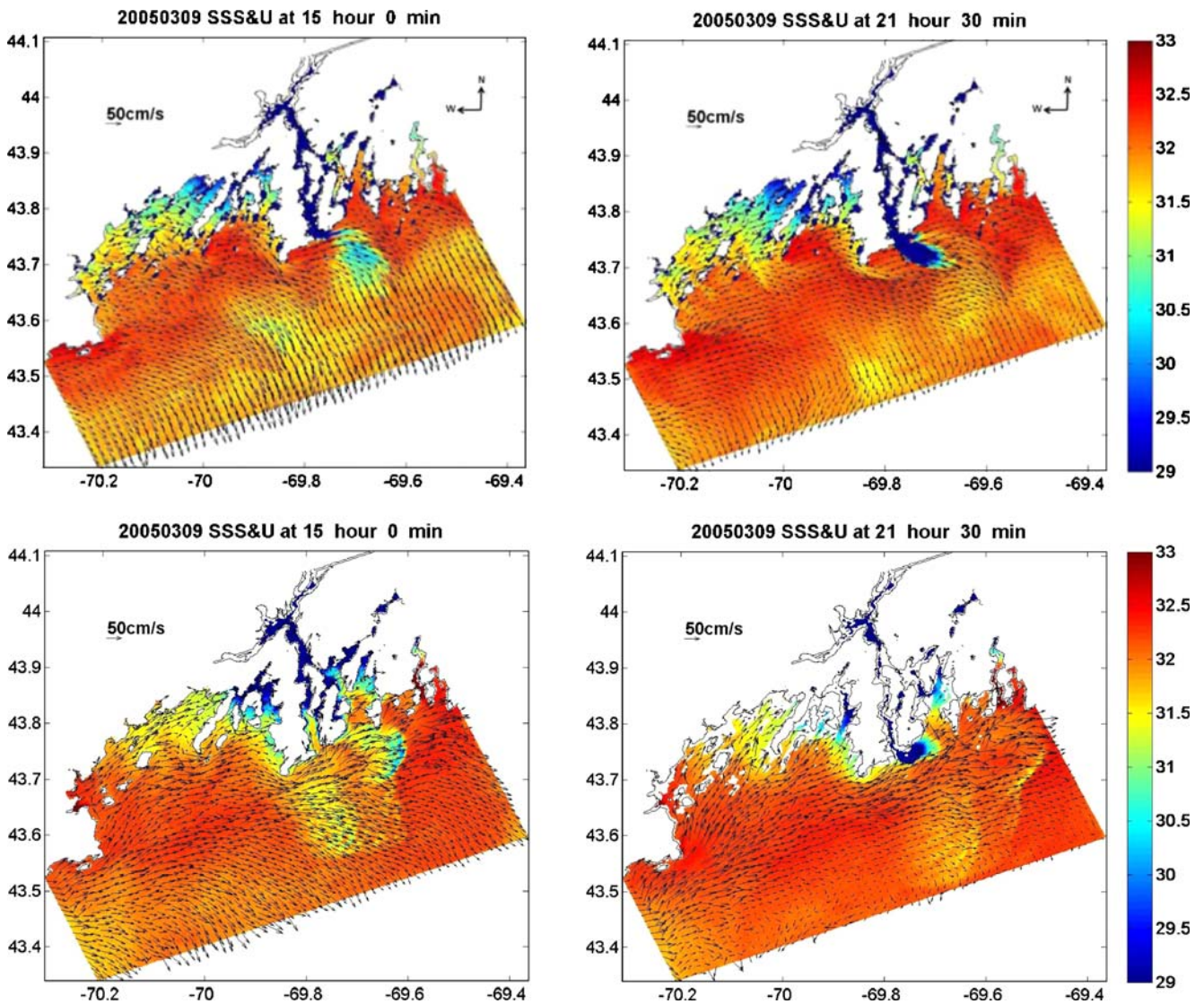


Fig. 12 Surface salinity and circulation patterns during the spring tides on 9 March 2005 at the highest (*left*) water level and the lowest (*right*) water level. The *upper* shows the model result without the WAD, whereas the lower shows the model result with the WAD

westerly wind on 9 March (Fig. 7e). Distortions could be identified in shallow areas of Casco Bay and the K–A estuary where the wet/dry conditions in these areas changed flow directions considerably. Flow directions were also different between the two experiments on the shelf. Moreover, the flow field was noisier in the experiment with WAD as seen clearly in Fig. 9.

5 Summary

This study focuses on the formation and evolution of the K–A river plume and the circulation of the Casco Bay region. Using a numerical model, we simulated the temporal/spatial variation of the salinity and temperature in response to the K–A river discharge and the meteorological forcing. The

modeled results agree with the observation from the mooring and shipboard surveys. The seasonal and the event scale variability as well as the spatial patterns in the salinity field from the coastal water to the estuary were favorably reproduced.

A new criterion using the surface salinity gradient was introduced to distinguish the plume from the ambient coastal water. The model results show that the plume expands in all directions after leaving the mouth. The calculated plume thickness suggests that the K–A plume is surface-trapped. Its horizontal scales are largely controlled by the discharge and they can be predicted using the linear relationships with $Q^{0.25}$. On the average, the down-coast, up-coast, and offshore extensions of the surface plume are 12, 8, and 8 km, respectively. The down-coast and offshore scales can grow much bigger, to ~30 km during peak

discharges. However, the up-coast scale seldom exceeds 16 km. The up-coast spreading is related to the orientation of the estuary mouth and the prevailing southwesterly wind in the summer. The upwelling favorable wind also transports the plume water offshore. The wind and tide help the surface plume water mix with the ambient coastal water and entrain the coastal water to form interleaving structures.

The Oey's WAD scheme (Oey 2005, 2006) is modified and implemented in the Casco Bay/K–A estuary model. The model mimics the flooding and ebbing processes in shallow areas. Also by comparing the model runs with and without the WAD, significant differences are found in the salinity distribution and the size of the plume. The WAD processes enhance the mixing and entrainment processes near the estuary, which results in stronger tidal intrusions into the estuary. Stronger mixing observed in the WAD case reduces the density gradients around the estuary mouth. The plume becomes thicker near the estuary mouth. The outflow velocity of the plume is weaker and the radius of the river plume shrinks. Although the circulation pattern generally agrees between the two model runs, the flow field in the run with the WAD is noisier, not only in shallow areas of Casco Bay but also in the plume and even on the shelf. The latter warrants further investigation. We speculate, however, that WAD processes can affect much larger areas than the intertidal zone especially via river plumes that feed into coastal currents.

Acknowledgments The authors would like to thank Dr. Joseph Salisbury of the Coastal Ocean Observing Center at the University of New Hampshire, Dr. Neal Pettigrew, and the GoMOOS buoy group for providing the cruise and mooring data used in this study. Two anonymous reviewers provided many valuable comments and suggestions, and their efforts are gratefully acknowledged. This study was supported by subcontracts of NASA Grant NNX08AC27G and NOAA Grant NA04NOS4780271 to the University of Maine.

References

- Avicola G, Huq P (2003) The characteristics of the recirculating bulge region in coastal buoyant outflows. *J Mar Res* 61:435–463
- Balzano A (1998) Evaluation of methods for numerical simulation of wetting and drying in shallow water flow models. *Coast Eng* 34:83–107
- Casco Bay Estuary project (1995) Draft Casco Bay plan. pp 217
- Chant RJ, Wilkin J, Zhang W, Choi B-J, Hunter E, Castelao R, Glenn S, Jurisa J, Schofield O, Houghton R, Kohut J, Frazer TK, Moline MA (2008) Dispersal of the Hudson River plume in the New York Bight: synthesis of observational and numerical studies during LaTTE. *J Oceanogr* 21:148–161
- Chao S-Y, Boicourt WC (1986) Onset of estuarine plumes. *J Phys Oceanogr* 16:2137–2149
- Choi B, Wilkin L (2007) The effect of wind on the dispersal of the Hudson River plume. *J Phys Oceanogr* 37:1878–1897
- Cousins, S, Xue H, Pettigrew N, Mickelson M (2006) Responses of the Gulf of Maine to Northeasters in May 2005—a case study using the GoMOOS nowcast/forecast System. Poster presented at the 2006 Ocean Sciences Meeting, Honolulu, HI
- Du Y (2008) Implementation of a wetting and drying model in simulating the Androscoggin/Kennebec plume and the circulation in Casco Bay. M.S. thesis, University of Maine, p 56
- Fong DA, Geyer WR, Signell RP (1997) The wind-forced response on a buoyant coastal current: observation of the west Maine coastal plume. *J Mar Syst* 12:69–81
- Fong DA, Geyer WR (2001) Response of a river plume during an upwelling favorable wind event. *J Geophys Res* 106:1067–1084
- Garvine RW (1987) Estuary plumes and fronts in shelf waters: a layer model. *J Phys Oceanogr* 17:1877–1896
- Garvine RW (1995) A dynamical system for classifying buoyant coastal discharges. *Cont Shelf Res* 15:1585–1596
- Garvine RW (2001) The impact of model configuration in studies of buoyant coastal discharge. *J Mar Res* 59:193–225
- Geyer WR, Signell RP, Fong DA, Wang J, Anderson DM, Keafer BA (2004) The freshwater transport and dynamics of the western Maine coastal current. *Cont Shelf Res* 24:1339–1357
- Hetland RD (2005) Relating river plume structure to vertical mixing. *J Phys Oceanogr* 35:1667–1688
- Hickey BM, Pietrafesa LJ, Jay DA, Boicourt WC (1998) The Columbia River plume study: subtidal variability in the velocity and salinity fields. *J Geophys Res* 103:10339–10368
- Hickey BM, Geier S, Kachel N, MacFadyen A (2005) A bi-directional river plume: the Columbia in summer. *Contl Shelf Res* 25:1631–1656
- Horner-Devine AR (2009) The bulge circulation in the Columbia River plume. *Cont Shelf Res* 29:234–251
- Janzen CD, Churchill JH, Pettigrew NR (2005) Observations of exchange between eastern Casco Bay and the western Gulf of Maine. *Deep-Sea Res II* 52:2411–2429
- Keafer BA, Churchill JH, Anderson DM (2005) Blooms of the toxic dinoflagellate, *Alexandrium fundyense* in the Casco Bay region of the western Gulf of Maine: advection from offshore source populations and interactions with the Kennebec River plume. *Deep-Sea Res II* 52:2631–2655
- Mellor GL, Yamada T (1982) Development of a turbulence closure model for geophysical fluid problems. *Rev Geophys Space Phys* 20:851–875
- Mellor GL (2002) Oscillatory bottom boundary layers. *J Phys Oceanogr* 32:3075–3088
- Mellor GL (2004) Users guide for a three-dimensional, primitive equation, numerical ocean model. Princeton University, Princeton, p 56
- Mendelsohn D, Yassuda E, Peene S (2001) A simplified method for marsh inundation modelling in hydrodynamic and water quality models with application to the Cooper river Estuary (SC). Proceedings of the 7th International Conference on Estuarine and Coastal Modelling, pp 654–669
- O'Donnell J (1990) The formation and fate of a river plume: a numerical model. *J Phys Oceanogr* 20:551–569
- Oey L (2005) A wetting and drying scheme for POM. *Ocean Model* 9:133–150
- Oey L (2006) An OGCM with movable land–sea boundaries. *Ocean Model* 13:176–195
- Oey L, Ezer T, Hu C, Muller-Karger FE (2007) Baroclinic tidal flows and inundation processes in Cook Inlet, Alaska: numerical modeling and satellite observations. *Ocean Dynamics* 57:205–221
- Parker CE (1982) The currents of Casco Bay and the prediction of oil spill trajectories. Technical report no. 28, Bigelow Laboratory for Ocean Sciences. Prepared for the State of Maine, State Planning Office.

- Pettigrew N, Churchill JH, Janzen CD, Mangum L, Signell RP, Thomas A, Townsend DW, Wallinga JP, Xue H (2005) The kinematic and hydrographic structure of the Gulf of Maine coastal current. *Deep-Sea Res II* 52:2369–2391
- Pinones A, Valle-Levinson A, Narvaez DA, Vargas CA, Navarrete SA, Yuras G, Castilla JC (2005) Wind-induced diurnal variability in river plume motion. *Estuar Coast Shelf Sci* 65:513–525
- Raineault NA (2006) Temporal and spatial variability of surface meteorological conditions over the Gulf of Maine: comparisons of the National Data Buoy Center observations and Eta model results. Honors thesis, University of Maine, p 38
- Uchiyama Y (2004) Wetting and drying scheme for POM and its application to San Francisco Bay. In: Cheng L, Yeow K (eds) *Hydrodynamics VI—theory and application*. Taylor & Francis Group, London, pp 293–299
- Xie L, Pietrafesa LJ, Peng M (2004) Incorporation of a mass-conserving inundation scheme into a three-dimensional storm surge model. *J Coast Res* 20:1209–1223
- Xue H, Shi L, Cousins S, Pettigrew NR (2005) The GoMOOS nowcast/forecast system. *Cont Shelf Res* 25:2122–2146
- Yankovsky A, Chapman DC (1997) A simple theory for the fate of buoyant coastal discharges. *J Phys Oceanogr* 27:1386–1401